Preliminary report on experiment CH6424

Summary

Four samples were measured, labelled as **tetrazol**, **MePy2**, **dabco** and **quinone**. Diffraction data for **MePy2** and **dabco** were measured up to 0.45 Å and were of high quality, so the charge densities were successfully refined (see below, Figs. 2-10). Crystals of **tetrazol** were small and twinned, which allowed only spheric refinement. Nevertheless, the atomic-resolution crystal structure is very accurate and publicable (see below, Table 1 and Fig. 1). Six high-resolution diffraction data of **quinone** were collected 0.45 Å, and spheric refinement was very good, yielding publicable crystal structures. However, multipolar refinement was difficult and residual density remains unacceptably high. We are still working on multipolar refinement; in the worst case, atomic-resolution crystal structure will be publicable.

Experimental

Single-crystal X-ray diffraction data were collected at the Rossendorf Beamline (ESRF / Grenoble, France) (Scheinost *et al.*, 2020) equipped with a Si(111) monochromator and two Pd coated mirrors. The single-crystal data were recorded with a Pilatus3 X 2M detector (Dectris) with an excitation energy of 20000 eV / 0.6200926 Å. The monochromator energy was calibrated against the first inflection of the *K*-absorption edge of a Mo metal foil point, tabulated as 20000 eV. The diffraction measurements were performed in shutterless mode with an angular step size of 0.1° and a counting time of 0.1s per frame. The detector geometry parameters were calibrated with *PyFAI* (Kieffer & Wright, 2013) using a powder pattern of the NIST 660b standard LaB_6. Experimental data were collected using the *Pylatus* software (Dyadkin *et al.*, 2016) and treated using the *SNBL ToolBox* (Dyadkin *et al.*, 2016) and *CrysAlisPro* (Rigaku OD, 2019).

The structures were solved using *SHELXT* (Sheldrick, 2018) and a spherical-atom model was refined using *SHELXL-2017* (Sheldrick, 2015). Multipolar refinement was carried out *vs*. all reflections F^2 with program package *MoPro* (Jelsch *et al.*, 2005). Metal and halogen atoms were modelled as hexadecapoles, O, N and C as octupoles and hydrogens as dipoles; loose

restraints were used for multipoles and exponential κ coefficients of chemically equivalent atoms. Vibrations of metal and halogen atoms were refined as anharmonic using fourth-order Gram-Charlier coefficients. Anisotropic parameters for hydrogen atoms were calculated by the *SHADE3* server (Madsen, 2006) and kept fixed in the multipolar atom refinement; aromatic C−H bond lengths were restrained to 1.077(2) Å and methyl C−H to 1.083(2) Å.

Due to a limited quality of the diffraction data and twinning, **tetrazol** was refined only by spheric model with resolution cut off to 0.80 Å.

For **Me2Py** and **dabco** resolution was cut off at 0.50 Å. In **Me2Py** vibrations of atoms N2B, C8B, N7, C14 and C25 were refined as anharmonic using fourth-order Gram-Charlier coefficients. In **dabco** vibrations of atoms C14A, and C16A were refined as anharmonic using fourth-order Gram-Charlier coefficients.

Geometry and charge-density calculations and analysis of Hirshfeld surfaces were performed by *MoPro* (Jelsch *et al.*, 2005); molecular graphics were prepared using *MoProViewer* (Guillot, 2012) and *CCDC-Mercury* (Macrae *et al.*, 2020). Crystallographic and refinement data are shown in Table 1.

Table 1 Crystallographic, data collection and charge-density refinement details.

Compound	**tetrazol**	**Me2Py**	**dabco**	**quinone***
Empirical formula	$C_{74}H_{42}N_{20}$	$C_{61}H_{31}N_{19}$	$C_{78}H_{59}N_{25}$	$C_{21}H_{11}Cl_5CuIN_3O_2$
Formula wt. / g mol^{-1}	1211.28	1029.97	1346.40	705.03
Crystal dimensions / mm	0.08 x 0.02 x 0.01	0.12 x 0.10 x 0.06	0.14 x 0.11 x 0.05	0.12 x 0.06 x 0.04
Space group	$P2_1/c$	$P\bar{1}$	$P\bar{1}$	$P\,2_1/n$
a / Å	29.0602(6)	13.1638(2)	7.8028(1)	9.90659(16)
b / Å	11.5161(3)	13.5312(2)	13.3989(1)	21.6589(4)
c / Å	19.7924(6)	15.6098(2)	16.5465(1)	17.4384(3)
α / °	90	105.985(1)	80.910(1)	90
β / °	109.859(3)	101.257(1)	81.4170(1)	140.309(3)
γ / °	90	103.275(1)	83.9710(1)	90
Z	4	2	2	4
V / Å^3	6229.8(3)	2500.30(6)	1683.175(17)	2389.58(7)
D_{calc} / g cm^{-3}	1.291	1.369	1.329	1.987

μ / mm^{-1}	0.053			2.830
θ range / °	1.52 – 40.67	1.47 – 40.49	1.46 – 40.61	1.48 – 35.51
T / K	100(2)	100(2)	100(2)	100(2)
Radiation wavelength	0.56356	0.56356	0.56356	0.56356
Detector type	Dectris Pilatus3 X 2M	Dectris Pilatus3 X 2M	Dectris Pilatus3 X 2M	Dectris Pilatus3 X 2M
Range of h, k, l	–66 < h < 66; –26 < k < 26; –45 < l < 45	–30 < h < 30; –26 < k < 26; –35 < l < 35	–18 < h < 17; –30 < k < 30; –37 < l < 38	–19 < h < 19; –43 < k < 43; –34 < l < 34
Reflections collected	439755	716861	253550	219444
Independent reflections	11124	36397	26904	19889
Reflections with $I \geq 2\sigma$	10370	27031	25613	15514
Absorption correction	multi-scan	multi-scan	multi-scan	multi-scan
T_{min}, T_{max}	multi-scan	0.891; 1.000	0.7422; 1.0000	0.6147; 1.0000
R_{int}	0.0758	0.0424	0.0288	0.0983
Spheric refinement				
Weighting scheme	$w = 1/[\sigma^2(F_o2)+(0.1701P)^2+8.6629P]$ where $P = (F_o^2+2F_c^2)/3$	$w = 1/[\sigma^2(F_o2)+(0.1533P)^2]$ where $P = (F_o^2+2F_c^2)/3$	$w = 1/[\sigma^2(F_o2)+(0.0866P)^2+0.605P]$ where $P = (F_o^2+2F_c^2)/3$	$w = 1/[\sigma^2(F_o2)+(0.0516P)^2+13.9368P]$ where $P = (F_o^2+2F_c^2)/3$
R (F)	0.0696	0.0752	0.0458	0.0864
R_w (F^2)	0.2250	0.2740	0.1398	0.2176
Goodness of fit	0.851	1.035	1.008	0.983
H atom treatment	Constrained isotropic	Constrained isotropic	Constrained isotropic	Constrained isotropic
No. of parameters	848	733	930	298
No. of restraints	0	9	9	0
$\Delta\rho_{max}$, $\Delta\rho_{min}$, $\Delta\rho_{rms}$ (e Å^{-3})	0.499; −0.384; 0.066	0.970; −1.298; 0.097	1.050; −1.050; 0.070	5.09; -5.32: 0.21

Multipolar refinement			
Weighting scheme	-	$w = 1/[\sigma^2(F_o^2)]$	$w = 1/[\sigma^2(F_o^2)]$
R (F)	-	0.0325	0.0216
R_w (F^2)	-	0.0645	0.0545
Goodness of fit	-	1.150	1.491
H atom treatment	-	Constrained anisotropic	Constrained anisotropic
No. of parameters	-	2141	2860
No. of restraints	-	1112	1351
$\Delta\rho_{max}$, $\Delta\rho_{min}$, $\Delta\rho_{rms}$ (e Å^{-3})	-	0.458; −0.609; 0.047	0.296; −0.283; 0.043

* The best data set so far. Two data sets still have to be integrated.

Crystal structure of *tetrazol*

Asymmetric unit of **tetrazol** (Fig. 1) containts two symmetry-independent tetrazolium cations and four symmetry-independent partially charged 7,7,8,8-tetracyanoquinodimethane (TCNQ) radical anions. From the stoichiometry, charge of TCNQ moieties is -1/2.

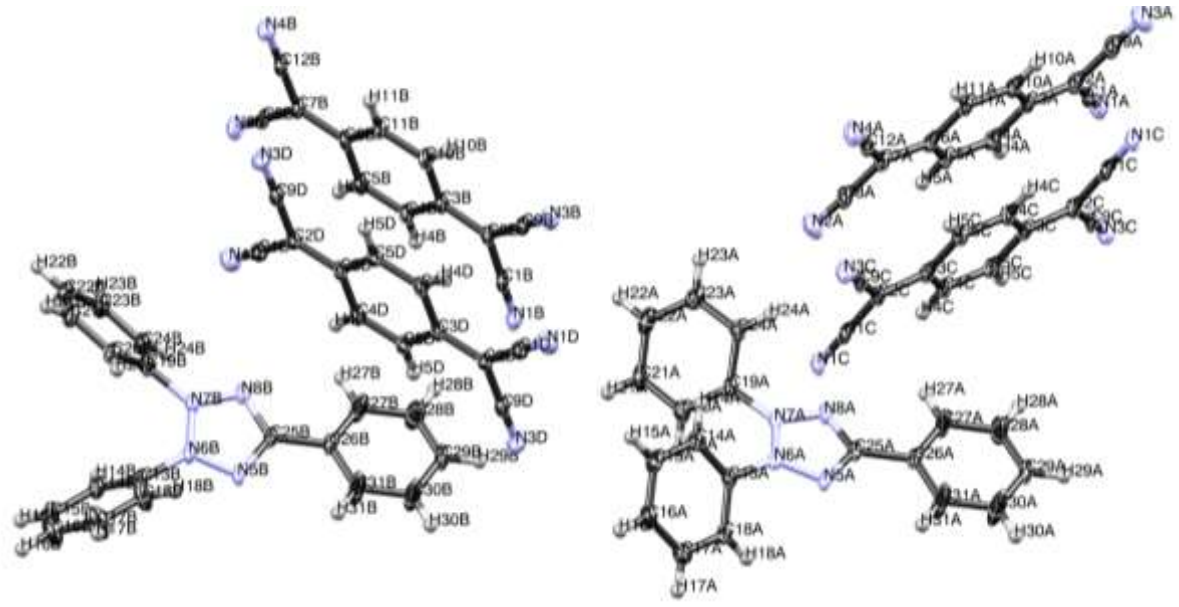

Figure 1 ORTEP drawing of asymmetric unit of **tetrazol** with atom labelling scheme. Displacement ellipsoids are drawn for the probability of 50 % and hydrogen atoms are shown as spheres of arbitrary radii.

Crystal structure and charge density of *Me2Py*

Asymmetric unit of **Me2Py** (Fig. 2) containts a 1,1'-methylenedipyridinium cation, four symmetry-independent partially charged 7,7,8,8-tetracyanoquinodimethane (TCNQ) radical anions and a solvent acetonitrile molecule. From the stoichiometry, charge of TCNQ moieties is -1/2.

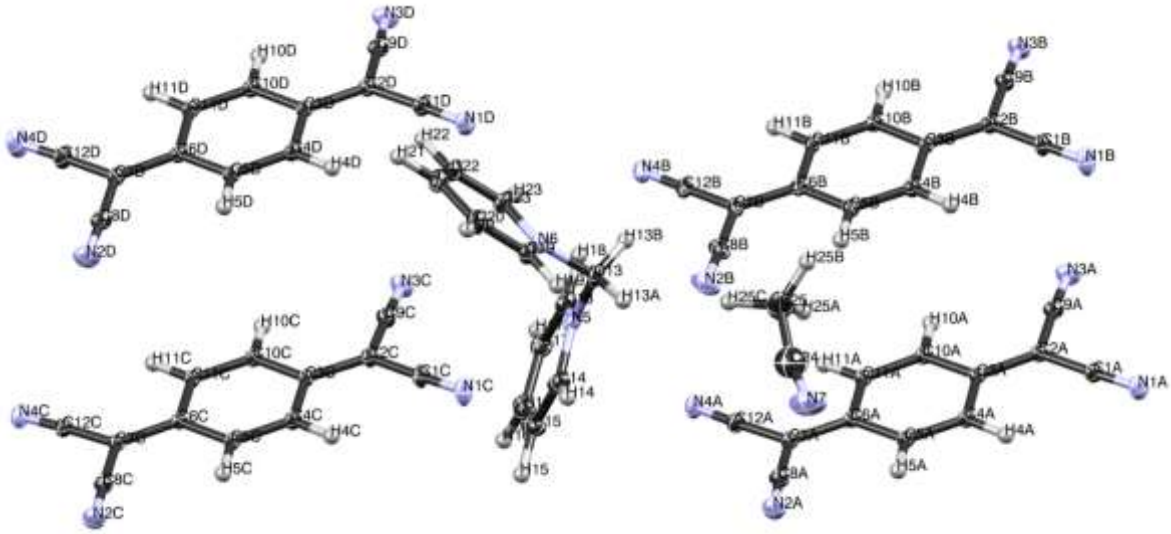

Figure 2 ORTEP drawing of asymmetric unit of **Me2Py** with atom labelling scheme. Displacement ellipsoids are drawn for the probability of 50 % and hydrogen atoms are shown as spheres of arbitrary radii.

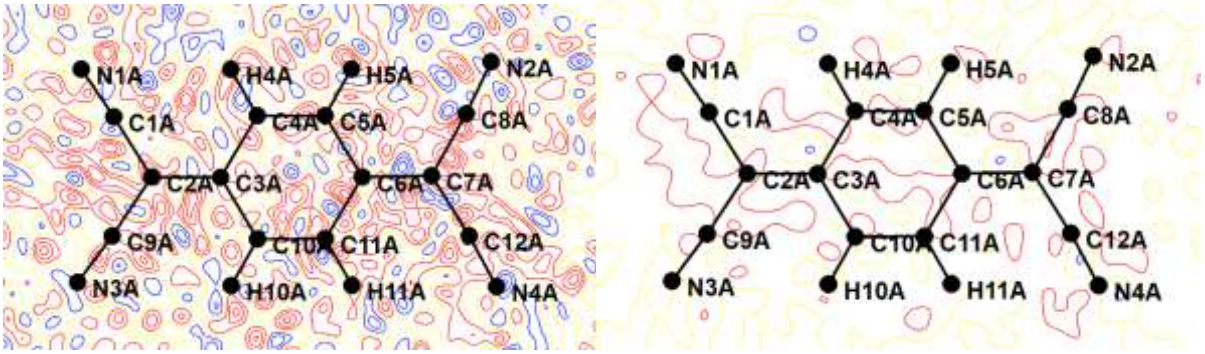

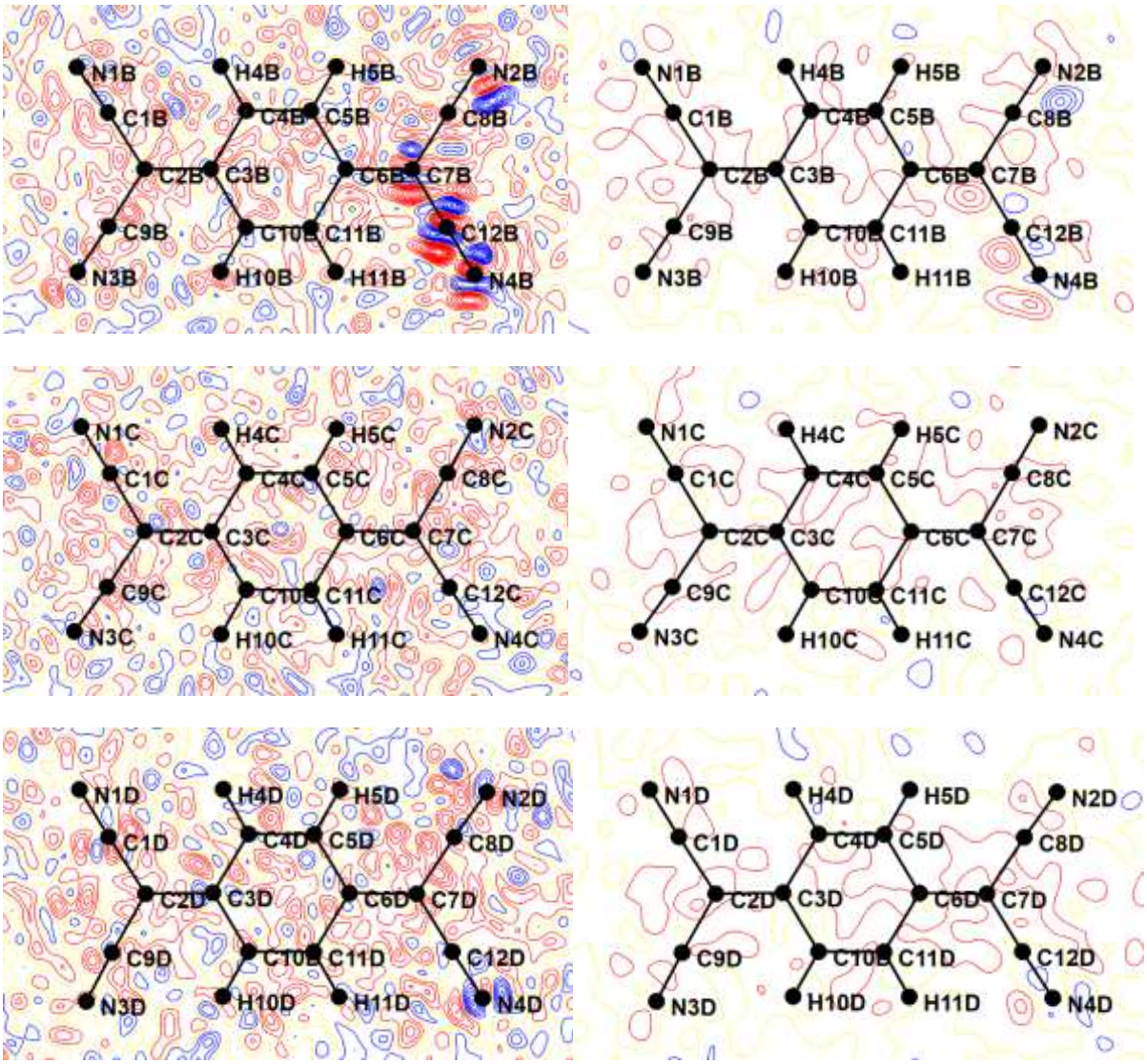

Figure 3 Residual density in the mean plane of four symmetry-independent TCNQ moieties in **Me2py** with all reflections used (left) and only low-angle reflections (sin θ / λ < 0.7 Å^{-1}) (right) used. Positive density is shown in blue and negative in red; yellow dotted lines represent zero density. The spacing between contours is of 0.05 eÅ^{-3}.

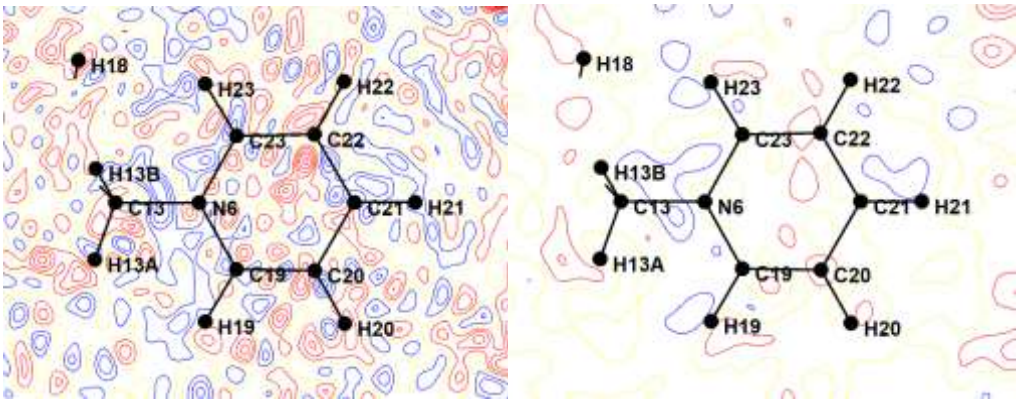

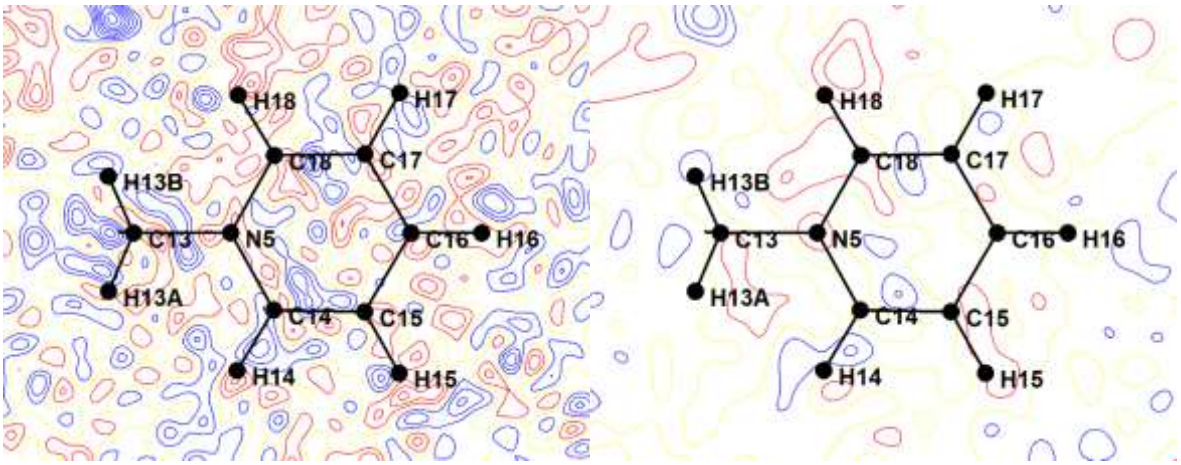

Figure 4 Residual density in the mean plane of two pyridinium rings of the cation in **Me2py** with all reflections used (left) and only low-angle reflections (sin θ / λ < 0.7 Å^{-1}) (right) used. Positive density is shown in blue and negative in red; yellow dotted lines represent zero density. The spacing between contours is of 0.05 eÅ^{-3}.

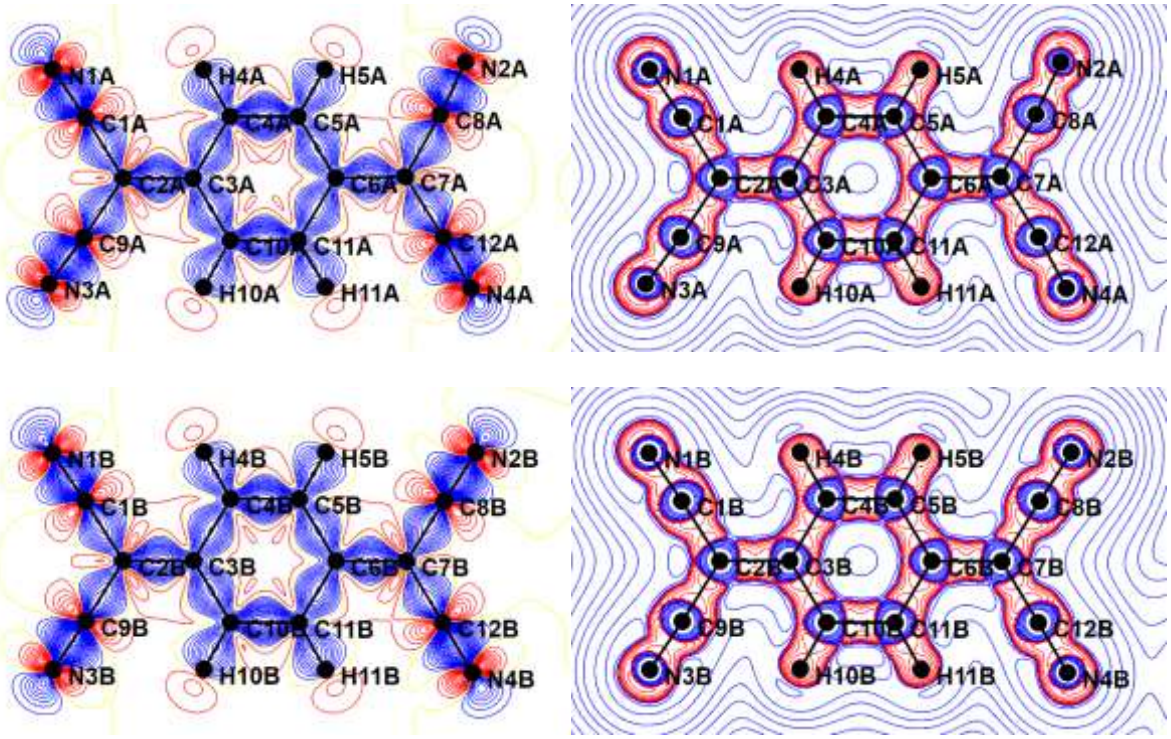

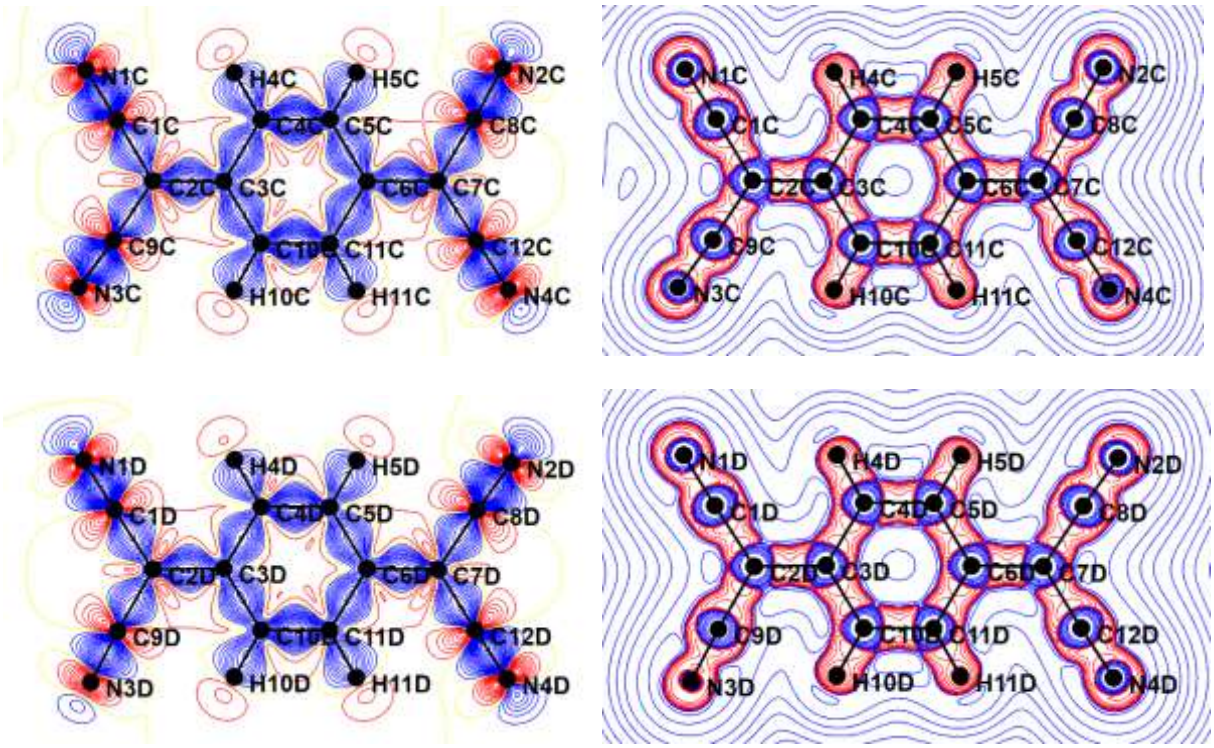

Figure 5 Left: deformation density maps in the mean planes of four symmetry-independent TCNQ moieties in **Me2py**. The spacing between contours is of 0.05 e Å^{-3}; the positive density is blue, the negative is red and the zero contour is drawn as a yellow dotted line. Right: Laplacians of electron density in the mean planes of four symmetry-independent TCNQ moieties in **Me2py**. The contours are drawn for 2, 4, 8·10^{n} e Å^{-5}, n = –3…2; positive Laplacian is blue and negative is red.

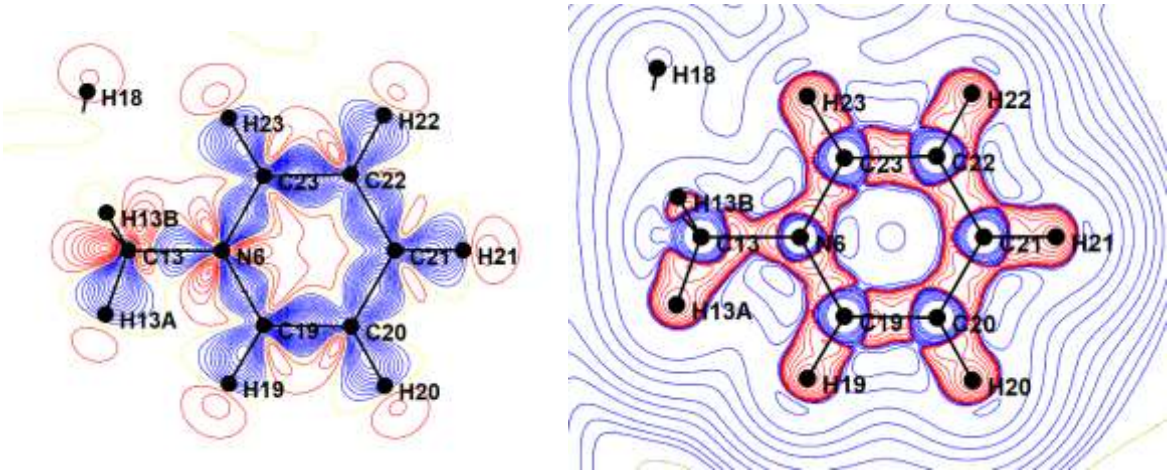

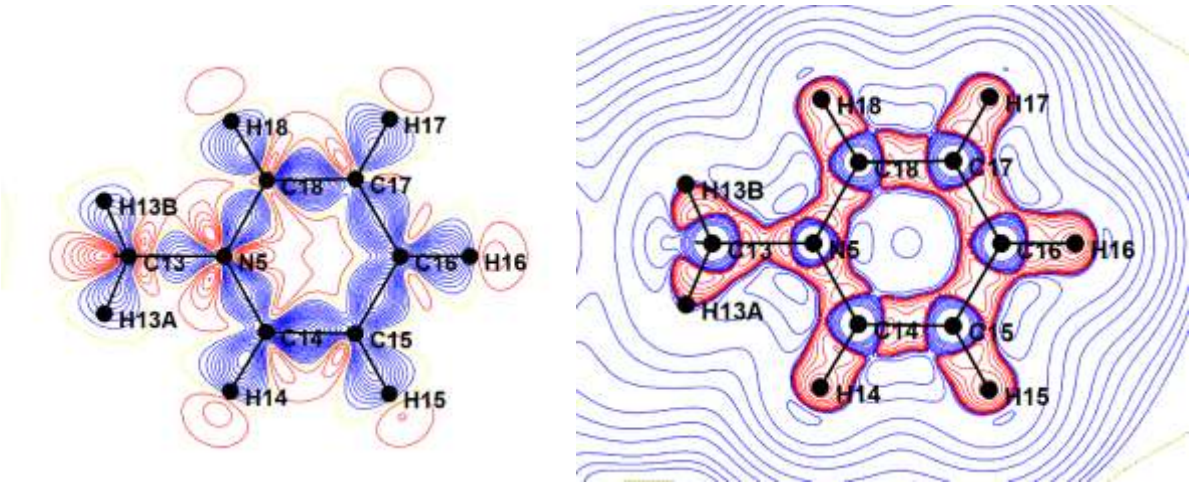

Figure 6 Left: deformation density maps in the mean planes of two pyridinium rings of the cation in **Me2py**. The spacing between contours is of 0.05 e Å^{-3}; the positive density is blue, the negative is red and the zero contour is drawn as a yellow dotted line. Right: Laplacians of electron density in the mean planes of two pyridinium rings of the cation. The contours are drawn for 2, 4, $8\cdot10^{n}$ e Å^{-5}, n = –3…2; positive Laplacian is blue and negative is red.

Crystal structure and charge density of *dabco*

Asymmetric unit of **dabco** (Fig. 7) containts two symmetry-independent *N*,*N*'-dimethyl-dabco cations, five symmetry-independent partially charged 7,7,8,8-tetracyanoquinodimethane (TCNQ) radical anions and a solvent acetonitrile molecule. From the stoichiometry, charge of four TCNQ moieties is -1/2, while the fifth one is neutral. With 103 symmetry-indepentent non-hydrogen atoms (and a total of 162 atoms), **dabco** may be the largest structure refined by unconstrained multipolar model so far.

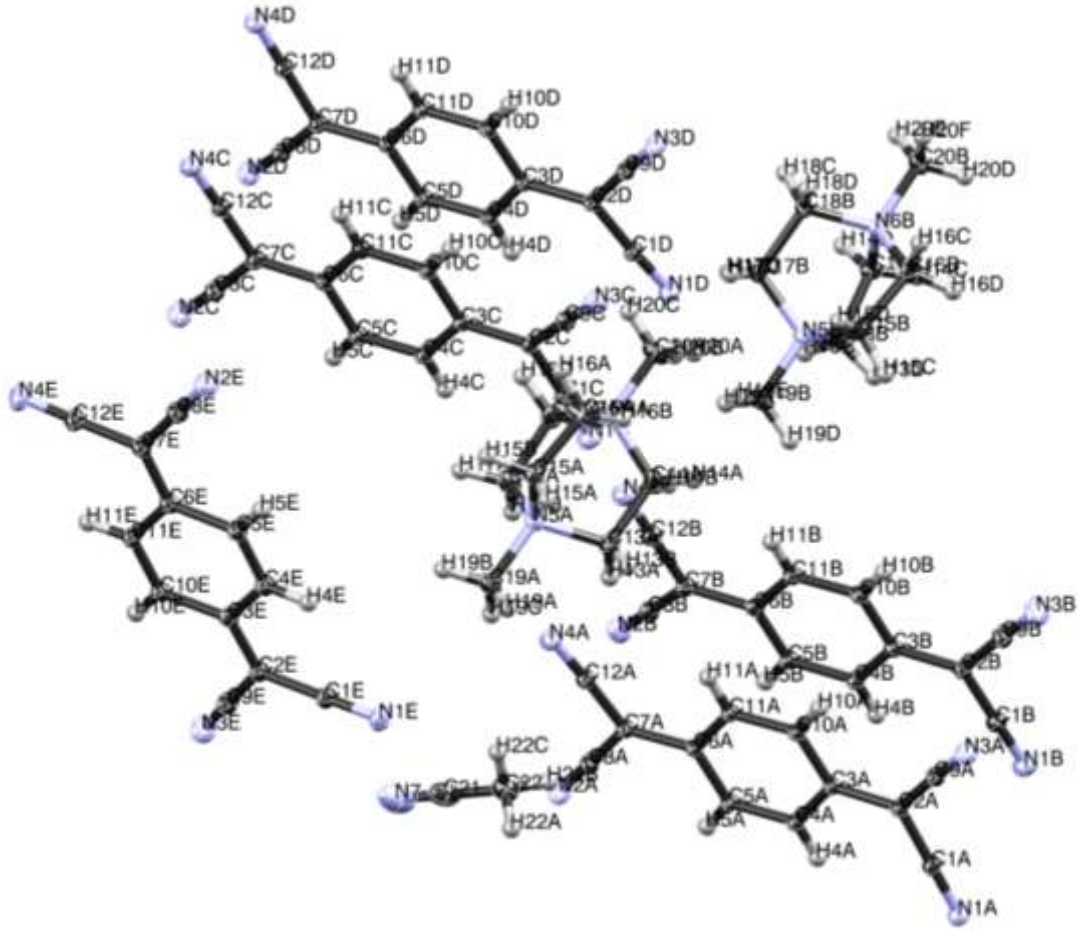

Figure 7 ORTEP drawing of asymmetric unit of **dabco** with atom labelling scheme. Displacement ellipsoids are drawn for the probability of 50 % and hydrogen atoms are shown as spheres of arbitrary radii.

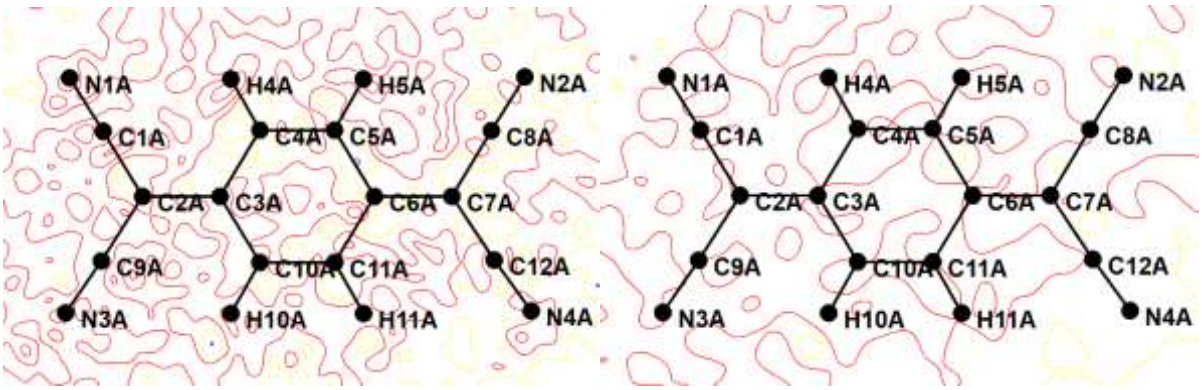

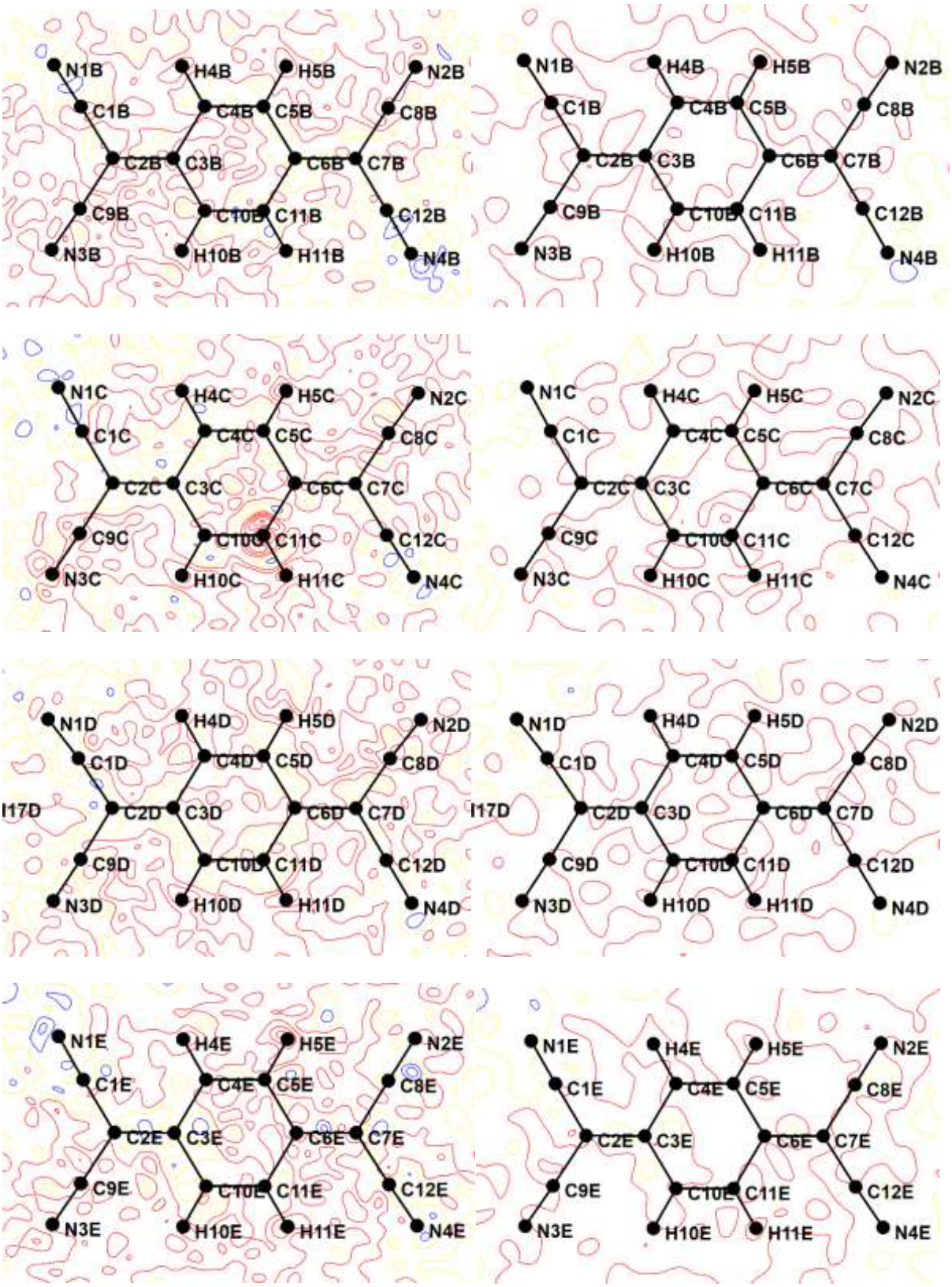

Figure 8 Residual density in the mean plane of five symmetry-independent TCNQ moieties in **dabco** with all reflections used (left) and only low-angle reflections (sin θ / λ < 0.7 Å^{-1}) (right) used. Positive density is shown in blue and negative in red; yellow dotted lines represent zero density. The spacing between contours is of 0.05 eÅ^{-3}.

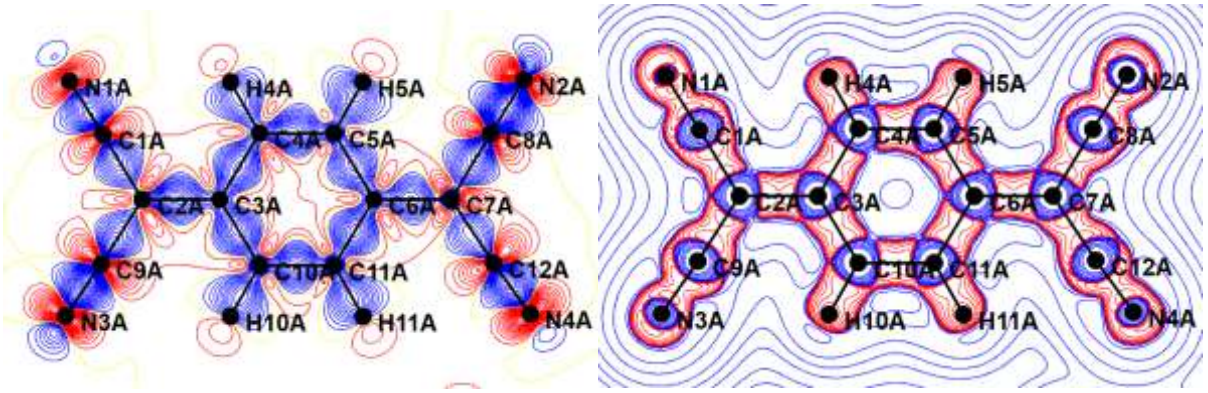
N1A
H4A
H5A
N2A
C1A
C4A
C5A
C8A
C2A
C3A
C6A
C7A
C9A
C10A
C11A
C12A
N3A
H10A
H11A
N4A

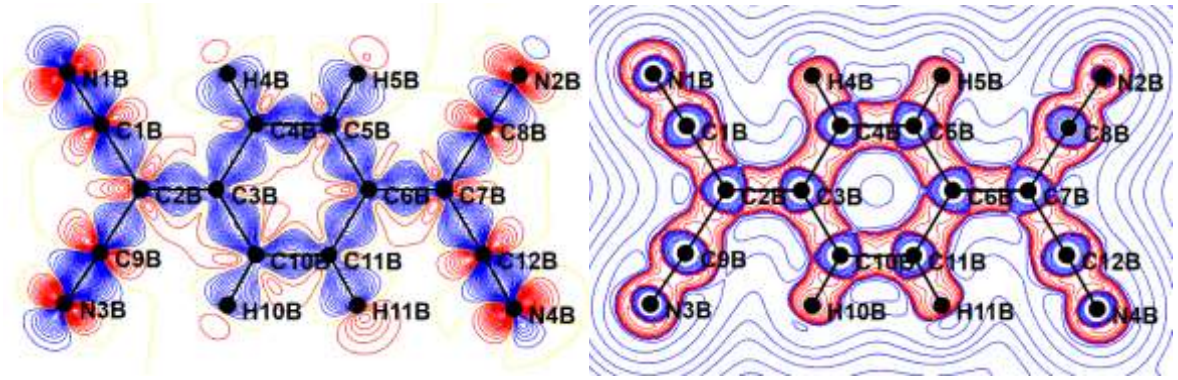
N1B
H4B
H5B
N2B
C1B
C4B
C5B
C8B
C2B
C3B
C6B
C7B
C9B
C10B
C11B
C12B
N3B
H10B
H11B
N4B

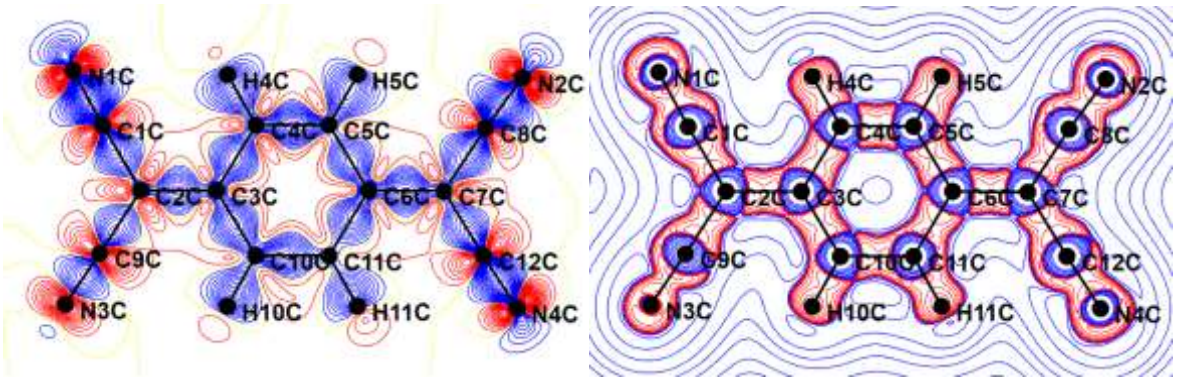
N1C
H4C
H5C
N2C
C1C
C4C
C5C
C8C
C2C
C3C
C6C
C7C
C9C
C10C
C11C
C12C
N3C
H10C
H11C
N4C

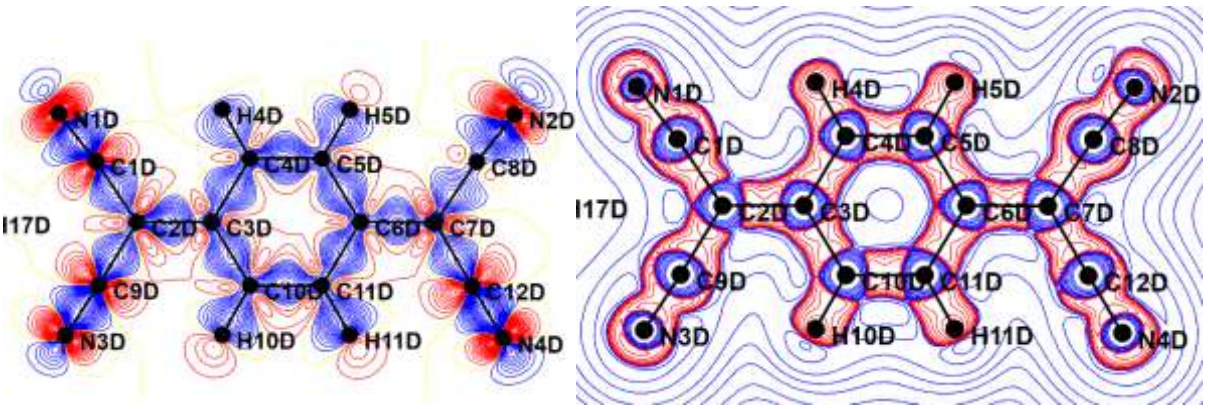
N1D
H4D
H5D
N2D
C1D
C4D
C5D
C8D
I17D
C2D
C3D
C6D
C7D
C9D
C10D
C11D
C12D
N3D
H10D
H11D
N4D

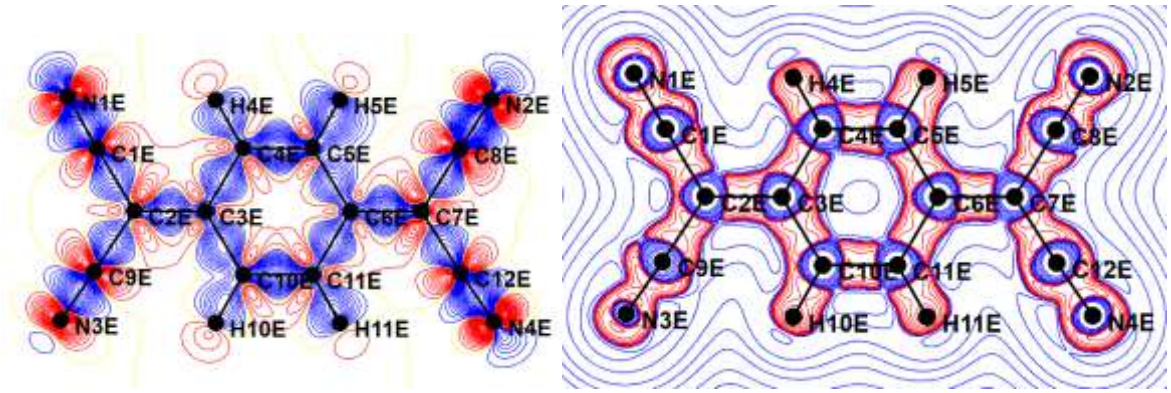

Figure 9 Left: deformation density maps in the mean planes of five symmetry-independent TCNQ moieties in **dabco**. The spacing between contours is of 0.05 e Å^{-3}; the positive density is blue, the negative is red and the zero contour is drawn as a yellow dotted line. Right: Laplacians of electron density in the mean planes of five symmetry-independent TCNQ moieties in **dabco**. The contours are drawn for 2, 4, 8·10^{n} e Å^{-5}, n = –3…2; positive Laplacian is blue and negative is red.

Crystal structure of *quinone*

Asymmetric unit of **quinone** (Fig. 10) comprises a molecule of a complex [CuICl(terpy)] (terpy = 2,2';6',2''-terpyridine) and a molecule of tetrachloroquinone.

So far, only four of six data sets have been processed and integrated. Spherical refinement of the best of them (Fig. 10) yielded *R* value of 8.64 % and maximum residual density of 5.09 e Å^{-3} using all data. With data cut off to atomic resolution, the maximum residual density is reduced below 2.0 e Å^{-3}, so the atomic resolution structure is publicable.

Multipolar refinement has not been completed, but so far it yielded unacceptably high residual density around the I1 atom of 5.07 e Å^{-3}. It will probably be improved, however, it is still not certain that the charge density would eventually be publicable.

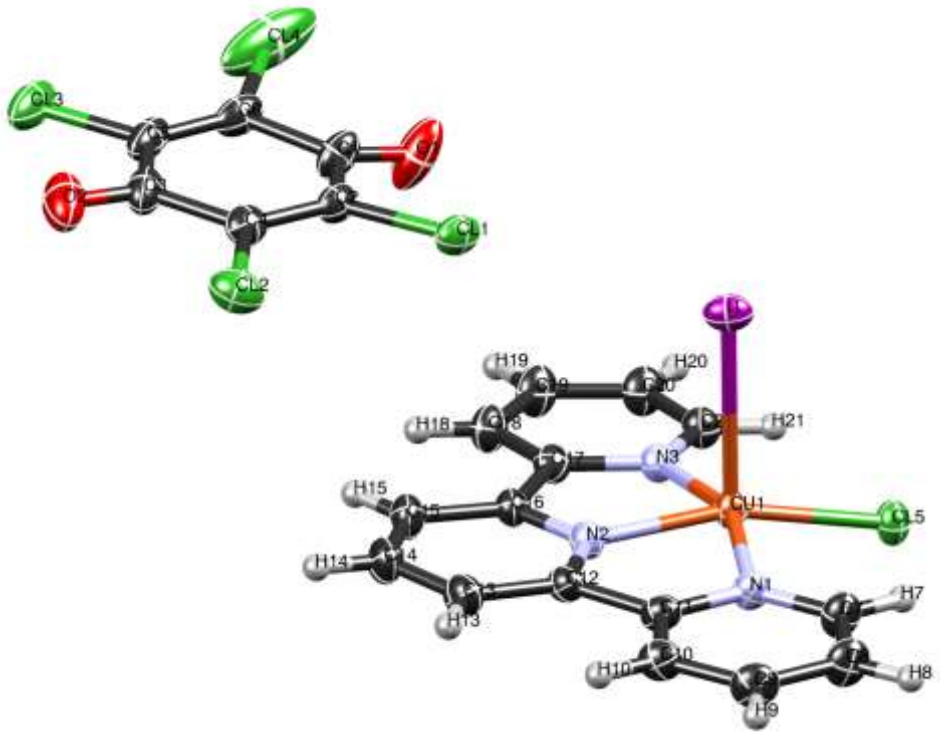

Figure 10 ORTEP drawing of asymmetric unit of **quinone** with atom labelling scheme. Displacement ellipsoids are drawn for the probability of 50 % and hydrogen atoms are shown as spheres of arbitrary radii.

References

Dyadkin, V.; Pattison, P.; Dimitiev V.; Chernyshov, D. (2016). *J. Synchrotron Rad*., **23**, 825-829.

Guillot, B. (2012). *Acta Crystallogr. A*, **68**, s204.

Jelsch, C.; Guillot, B.; Lagoutte, A.; Lecomte, C. (2005). *J. Appl. Crystallogr.*, **38**, 38-54.

Kieffer J.; Wright, J.P. (2013). *Powder Diffraction*, **28** (S2), 339-350.

Macrae, C. F., I. Sovago, S. J. Cottrell, P. T. A. Galek; McCabe, P.; Pidcock, E.; Platings, M.; Shields, G. P.; Stevens, J. S.; Towler, M. & Wood, P. A. (2020). *J. Appl. Cryst.* **53**, 226–235.

Madsen, A. Ø. (2006). *J. Appl. Cryst.*, **39**, 757-758.

Rigaku OD (2019). Crysalis Pro V.40 Rigaku Oxford diffraction.

Scheinost, A. C.; Claussner, J.; Exner, J.; Feig, M.; Findeisen, S.; Hennig, C.; Kvashnina, K. O.; Naudet, D.; Prieur, D.; Rossberg, A.; Schmidt, M.; Qiu, C.; Colomp, P.; Cohen, C.; Dettona, E.; Dyadkin, V.; Stumpf T. (2020). *J. Synchr. Rad*., **28**, 333-349.

Sheldrick, G. M. (2015). *Acta Cryst*. **C71**, 3–8.

Sheldrick, G. M. (2018). *Acta Crystallogr. A*, **A71**, 3-8.